Available online at www.sciencedirect.com
ScienceDirect
Journal of Magnetic Resonance 184 (2007) 62–71
JMR Journal of Magnetic Resonance
www.elsevier.com/locate/jmr

How accurately can the parameters from a model of anisotropic ^{3}He gas diffusion in lung acinar airways be estimated? Bayesian view

Alexander L. Sukstanskii [a,*], G. Larry Bretthorst [a], Yulin V. Chang [b], Mark S. Conradi [a,b], Dmitriy A. Yablonskiy [a,b]

[a] *Department of Radiology, Washington University, St. Louis, MO 63110, USA*
[b] *Department of Physics, Washington University, St. Louis, MO 63110, USA*

Received 14 June 2006; revised 21 September 2006
Available online 9 October 2006

Abstract

In the framework of a recently proposed method for *in vivo* lung morphometry, acinar lung airways are considered as a set of randomly oriented cylinders covered by alveolar sleeves. Diffusion of ^{3}He in each airway is anisotropic and can be described by distinct longitudinal and transverse diffusion coefficients. This macroscopically isotropic but microscopically anisotropic model allows estimation of these diffusion coefficients from multi *b*-value MR experiments despite the airways being too small to be resolved by direct imaging. Herein a Bayesian approach is used for analyzing the uncertainties in the model parameter estimates. The approach allows evaluation of relative errors of the parameter estimates as functions of the "true" values of the parameters, the signal-to-noise ratio, the maximum *b*-value and the total number of *b*-values used in the experiment. For a given set of the "true" diffusion parameters, the uncertainty in the estimated diffusion coefficients has a minimum as a function of maximum *b*-value and total number of data points. Choosing the MR pulse sequence parameters corresponding to this minimum optimizes the diffusion MR experiment and gives the best possible estimates of the diffusion coefficients. The mathematical approach presented can be generalized for models containing arbitrary numbers of estimated parameters.

Keywords: Diffusion MRI; Hyperpolarized gas; Lung airways; Bayesian analysis

1. Introduction

Emphysema, which is one of the leading causes of death in industrialized countries, is characterized by "abnormal, permanent enlargement of air spaces distal to the terminal bronchioles, accompanied by destruction of their walls, without fibrosis" [1]. An accurate characterization of emphysema requires diagnostic methods that are non-invasive and sensitive to the *regional lung microstructure at the alveolar level* in the living lung. Diffusion MR lung imaging with hyperpolarized ^{3}He gas has a potential to provide this sensitivity. Measurements of mean apparent diffusion coefficient (ADC) of ^{3}He gas for short (on the order of few milliseconds) diffusion times [2–9] and long (on the order of seconds) diffusion times [10–13] demonstrated substantial ADC changes with the progression of emphysema. Moreover, in a previous publication [5], we have proposed a method for *in vivo* lung morphometry, which is based on evaluation of anisotropic diffusion of hyperpolarized ^{3}He gas in acinar lung airways. The method allows quantitative analysis of the geometrical parameters describing the acinar airways and reveals a substantial difference between those in healthy and emphysematous lungs.

In any medium the atoms or molecules diffuse; that is, the atoms perform a Brownian-motion random walk. In

* Corresponding author. Fax: +1 314 362 0526.
E-mail address: alex@wuchem.wustl.edu (A.L. Sukstanskii).

1090-7807/$ - see front matter © 2006 Elsevier Inc. All rights reserved.
doi:10.1016/j.jmr.2006.09.019

time interval Δ, in the absence of restricting barriers the molecules typically sample a root mean-square distance $l_0 = (2D_0\Delta)^{1/2}$ along any axis. The parameter D_0 is termed the free diffusion coefficient, which for ^{3}He at infinite dilution in air at 37 °C is $D_0 = 0.88$ cm^2/s. Hence ^{3}He gas atoms can wander distances on the order of 1 mm in times as short as 1 ms. In lungs, the alveolar walls, the walls of bronchioles, the alveolar ducts, sacs and other branches of the airway tree serve as obstacles to the path of diffusing atoms and reduce the diffusion displacement. The above displacement estimate indicates that ^{3}He atoms can wander the length of several alveoli during the typical MR diffusion measurement of several milliseconds. Therefore, the main geometrical units considered in the model [5] are not individual alveoli but rather cylindrical airways covered by alveolar sleeves. Such a model was first introduced and histologically evaluated to characterize the geometry of acinar airways in human lungs [14]. Gas motion along the axis of an airway is less restricted than perpendicular to the axis; thus, diffusion in the lung is *anisotropic* and can be described by two different diffusion coefficients—longitudinal (along cylinder axis), D_L, and transverse, D_T, with $D_L > D_T$. This anisotropy was shown to manifest itself in the MRI signal even though each imaging voxel contains a very large number of differently oriented airways that cannot be resolved by direct imaging. In particular, this "microscopic" anisotropy of diffusion results in non-exponential MR signal decay as a function of b-value of the diffusion-sensitizing gradient. The diffusion coefficients D_L and D_T were estimated from the MR signal data at several b-values by using Bayesian probability theory. Computer simulations of ^{3}He gas diffusion in alveolar ducts [15] demonstrated a good agreement with results of our model. Knowing the transverse diffusion coefficient D_T and its relationship with the mean airway radius R, derived in [5] for a specific diffusion-sensitizing pulse gradient waveform, the mean acinar airway radius R was also estimated. A dependence of longitudinal diffusivity on the geometrical structure of acinar airways can also be estimated numerically using previously proposed expansile alveolar duct model [16,17].

The proposed method [5] has shown a great potential for evaluation of emphysema. Herein we present a theoretical analysis of uncertainties in parameter estimates inherent to this approach. We derive expressions for relative errors of the estimates as functions of "true" values of the parameters, signal-to-noise ratio, the maximum b-value and total number of b-values used in the experiment. As shown below, for a given set of the "true" diffusion parameters, the dependences of the relative errors of the diffusion coefficients on the maximum b-value and total number of data points (b-values) have minima. Choosing the MR pulse sequence parameters corresponding to these minima optimizes the diffusion MR experiment and gives the best possible estimates of the diffusion coefficients, providing that the signal-to-noise ratio is sufficiently high to ensure the signal remains higher than the noise level.

2. Theory

In the model, lung acinar airways are approximated by cylinders oriented uniformly in all directions (isotropic on the voxel scale). The ^{3}He gas diffusion-attenuated signal S as a function of the b-value depends on three parameters: the longitudinal and transverse diffusion coefficients D_L and D_T (or their linear combination) and the unattenuated signal amplitude S_0 [5]:

$$S(b) = S_0 \exp(-bD_T)\left(\frac{\pi}{4bD_A}\right)^{1/2} \cdot \Phi\left[(bD_A)^{1/2}\right], \tag{1}$$

where $D_A = D_L - D_T$ is the diffusion anisotropy and $\Phi(x)$ is the error function.

In our previous study [5], the model function (1) and Bayesian probability theory were used to estimate the diffusion coefficients D_L and D_T from the MR signal data at several b-values. As shown by Bretthorst [18,19], the Bayesian approach can also be used to analyze how the parameter estimates depend on their "true" values, signal-to-noise ratio, data sampling and total number of data values. In what follows, we will use this approach to analyze the uncertainty in the estimates of the parameters S_0, D_A, and D_T (we chose the diffusion anisotropy D_A rather than the longitudinal diffusion coefficient D_L for the third parameter, for convenience).

The basic quantity in this analysis is the joint posterior probability, $P(\{p_j\}|D\sigma I)$, for the model parameters $\{p_j\}$ given all of the data D, the prior information I and the standard deviation of the prior probability of the noise, σ. In a high signal-to-noise approximation, the joint posterior probability can be represented in the form [18,19]:

$$P(\{p_j\}|D\sigma I) \propto \exp\left(-\frac{Q}{2\sigma^2}\right), \tag{2}$$

where

$$Q = \sum_{n=0}^{N-1}\left[\hat{S}(b_n) - S(b_n)\right]^2. \tag{3}$$

Here $S(b_n)$ depends on the model parameters $\{p_j\} = \{S_0, D_A, D_T\}$ according to Eq. (1); $\hat{S}(b_n)$ is determined by the same Eq. (1) with substitution $\{S_0, D_A, D_T\} \to \{\hat{S}_0, \hat{D}_A, \hat{D}_T\}$, where $\hat{S}_0$, $\hat{D}_A$, and $\hat{D}_T$ are the "true" values of these parameters. The sum in Eq. (3) is over the N evenly spaced b-values, $b_n = n \cdot \Delta b$, $n = 0, 1, \ldots, N-1$. The maximum b-value is $b_{max} = \Delta b \cdot (N-1)$. Generally speaking, our analysis can be generalized for an arbitrary set of the b-values (e.g., irregularly spaced b-values, repeated b-values, etc.); however, we restrict our analysis to the evenly spaced set of b-values, for which relatively simple analytical expressions for the parameter estimates can be obtained.

In what follows, we denote the three parameters appearing in the model (1) as $p_S = S_0$, $p_A = D_A$ and $p_T = D_T$. The marginal posterior probability, represented symbolically as $P(p_j|D\sigma I)$, for each of the parameter p_j can be obtained by

integrating the joint posterior probability $P(\{p_j\}|D\sigma I)$ over the two other parameters:

$$P(p_j|D\sigma I) \propto \int\int \left(\prod_{i\neq j} \mathrm{d}p_i\right) P(\{p_j\}|D\sigma I) \propto \int\int \left(\prod_{i\neq j} \mathrm{d}p_i\right) \exp\left(-\frac{Q}{2\sigma^2}\right) \quad (4)$$

(hereafter all constants which cancel with normalization are omitted).

The multiple integrals in Eq. (4) can be evaluated numerically. Generally, the probability distributions $P(p_j|D\sigma I)$ obtained may have rather complicated structure (see examples in Section 4). However, in the case of high signal-to-noise ratio, the problem can be substantially simplified because the integrand in Eq. (4) has a sharp maximum with respect to all the arguments and the integrations in Eq. (4) can be therefore evaluated in the Laplace approximation (see details in Appendix; the validity of this approximation is discussed in Section 4):

$$P(p_j|D\sigma I) \propto \exp\left(-\frac{(p_j-\hat{p}_j)^2}{2\sigma_j^2}\right), \quad (5)$$

where σ_j is the width of the posterior probability distribution of the parameter p_j,

$$\sigma_j = \varepsilon_j \hat{p}_j, \qquad \varepsilon_j = \frac{1}{\mathrm{SNR}} \cdot U_j(\hat{D}_\mathrm{A}, \hat{D}_\mathrm{T}, \Delta b, N). \quad (6)$$

Here ε_j is the relative error of the parameter estimate, $\mathrm{SNR} = \hat{S}_0/\sigma$ is the signal-to-noise ratio of the attenuated signal. Explicit expressions for the functions $U_j(\hat{D}_\mathrm{A}, \hat{D}_\mathrm{T}, \Delta b, N)$ are given in Appendix, Eqs. (23)–(25). The estimates (mean ± standard deviation) of the parameters p_j are given by

$$(p_j)_{\mathrm{est}} = \hat{p}_j \pm \sigma_j = \hat{p}_j(1 \pm \varepsilon_j). \quad (7)$$

The expressions for σ_j and ε_j can be equally well represented in terms of other combinations of the diffusion parameters, for instance, $\hat{D}_\mathrm{L}, \hat{D}_\mathrm{T}$ or $\hat{D}_\mathrm{A}$ and the mean diffusivity $\hat{D}_\mathrm{M} = (\hat{D}_\mathrm{L} + 2\hat{D}_\mathrm{T})/3$. These expressions can also be written in the form of Eqs. (6); the difference will be only in the structure of the functions I_{ik} in Eqs. (19)–(21) entering the functions U_j. As expected, the values of ε_j are independent of the choice of the parameter set used for the calculations.

If the b-value increment Δb is small enough so that $\Delta b \cdot \hat{D}_\mathrm{T} < 1$, $\Delta b \cdot \hat{D}_\mathrm{A} < 1$ as generally occurs, the expressions for ε_j can be simplified and re-written in the form

$$\varepsilon_j = \frac{1}{\mathrm{SNR} \cdot \sqrt{N}} \cdot V_j(B_\mathrm{A}, B_\mathrm{T}), \quad (8)$$

where the functions $V_j(B_\mathrm{A}, B_\mathrm{T})$ depend only on two dimensionless parameters $B_\mathrm{A} = b_{\max}\hat{D}_\mathrm{A} \cdot N/(N-1)$, $B_\mathrm{T} = b_{\max}\hat{D}_\mathrm{T} \cdot N/(N-1)$. For sufficiently large N and fixed $b_{\max}$, the arguments to the functions V_j become independent of N and the relative errors ε_j turn out to be inversely proportional to $\sqrt{N}$.

Eqs. (6) or (8) allow calculation of the uncertainty of the parameter estimates at given values of the "true" parameters $\{\hat{S}_0, \hat{D}_\mathrm{A}, \hat{D}_\mathrm{T}\}$, Δb, SNR and N. For standard ^{1}H imaging SNR and N are independent parameters. However, hyperpolarized ^{3}He gas imaging is profoundly different from ^{1}H imaging because the longitudinal spin polarization of ^{3}He atoms does not recover after being flipped. This is not a problem in some animal experiments where data are acquired with multiple boluses of ^{3}He gas. In most human studies, however, hyperpolarized ^{3}He diffusion imaging experiments are performed in one short breathhold, using a fixed bolus of gas to yield all N images. This approach also insures better reproducibility of measurements as it provides for a relatively fixed state of lung inflation [8]. A larger number N of b-values requires use of a smaller flip angle, the latter being inversely proportional to $\sqrt{N}$ [20], in the nearly always applicable small flip angle approximation. As a result, the signal amplitude and, correspondingly, SNR turn out also to be inversely proportional to $\sqrt{N}$, and Eq. (6) should be modified by the substitution

$$\mathrm{SNR} \to \mathrm{SNR}_0/\sqrt{N}, \quad (9)$$

where SNR_0 denotes the signal-to-noise ratio of the unattenuated signal with the flip angle optimized for $N = 1$. The expressions for the relative errors calculated with such a substitution (hereafter denoted as ε'_j) take the form

$$\varepsilon'_j = \frac{\sqrt{N}}{\mathrm{SNR}_0} \cdot U_j(\hat{D}_\mathrm{A}, \hat{D}_\mathrm{T}, \Delta b, N). \quad (10)$$

In the case $\Delta b \cdot \hat{D}_\mathrm{T} < 1$, $\Delta b \cdot \hat{D}_\mathrm{A} < 1$, Eq. (10) reduces to

$$\varepsilon'_j = \frac{1}{\mathrm{SNR}_0} \cdot V_j(B_\mathrm{A}, B_\mathrm{T}) \quad (11)$$

and for sufficiently large N and fixed $b_{\max}$, the ε'_j become independent of N.

3. Results

The expressions derived in our study allow analysis of how the uncertainties in the parameter estimates depend on the experimental settings. The dependence of the ε_j on SNR (or SNR_0 for ε'_j) is similar to the $1/SNR$ dependence of the standard deviation of the ADC, obtained in the framework of the monoexponential model in [21]. Note however, that this result is valid only for high SNR, when the Laplace approximation used in deriving Eq. (6) is applicable (see Section 5).

The dependences of the relative errors on the maximum b-value, $b_{\max} = \Delta b \cdot (N-1)$ (with number of data points N fixed), are shown in Fig. 1a for fixed $\mathrm{SNR} = 100$, $N = 6$, $\hat{D}_\mathrm{L} = 0.4\ \mathrm{cm}^2/\mathrm{s}$, and $\hat{D}_\mathrm{T} = 0.1\ \mathrm{cm}^2/\mathrm{s}$. These values of the diffusion coefficients are typical for healthy human lungs; hereafter they will be used as default. For clarity, the ε_j cor-

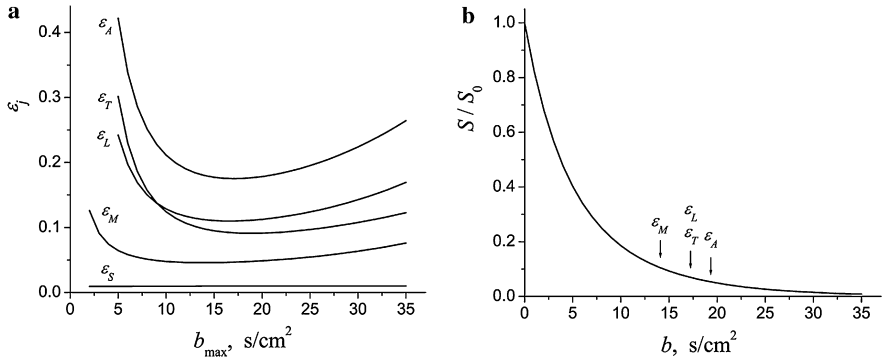

Fig. 1. (a) The relative errors ε_j as functions of the maximum b-value, b_{max}, for a fixed number $N = 6$ of data points. (b) The signal S, Eq. (1), as a function of the b-value. The default values of the parameters are assumed. The arrows on the decay curve indicate values of b at which each of the errors ε_j on the panel (a) are minimum.

responding to the parameters S_0, D_L, D_T, D_A, and D_M are denoted ε_S, ε_L, ε_T, ε_A, and ε_M, respectively.

As seen in Fig. 1a, all the relative errors except ε_S as functions of b_{max} have broad minima. In general, the positions of these minima depends on the "true" values of the diffusion parameters and the number N of data points (for the default values of the parameters and $N = 6$, the minima occur at $b_{max} = 14$ s/cm^2 for ε_M, at $b_{max} = 17$ s/cm^2 for ε_A and ε_L, and at $b_{max} = 19$ s/cm^2 for ε_T). The relative error ε_S corresponding to the unattenuated signal amplitude S_0 is practically independent of b_{max}, because the estimated S_0 value comes primarily from the $b = 0$ datum. In Fig. 1b we show the signal decay with increasing b-value for the same default diffusion parameters, calculated according to Eq. (1) (solid curve); the arrows mark the positions of the minima of the corresponding relative errors ε_j. Although the minima for ε_j are achieved at rather high b-values, the signal S may still remain above the noise level (due to the slower than exponential dependence of signal on bD_A in Eq. (1); see the arrows in Fig. 1b). The signal at the b-values for the minima of ε_j is about 5–10% of its initial value and is substantially higher than the noise level for the case considered (SNR = 100).

The dependences of the ε_j on the number of data points N (with b_{max} fixed) are demonstrated in Fig. 2 by the dotted lines. Fig. 2a corresponds to the case when the SNR is independent of N and the ε_j are determined by Eq. (6). Fig. 2b corresponds to the case (relevant to hyperpolarized gas experiments as performed currently with a single bolus of gas for all N images) when the SNR is inversely proportional to $\sqrt{N}$, the ε'_j are determined by Eq. (10).

In Fig. 2a, the relative errors monotonically decrease with N, being proportional to $1/\sqrt{N}$ for sufficiently large N (as follows from Eq. (8)). In Fig. 2b, the relative errors ε'_j calculated in the case when the SNR is inversely proportional to $\sqrt{N}$, all the relative errors (except ε'_S) have broad minima and tend to constant values at large N. The positions of these minima depend on b_{max}; for the default values of the diffusion parameters and $b_{max} = 10$ s/cm^2 (this value of b_{max} is typical for our experiments [5]; see also Section 5), the minima of all the relative errors ε'_j are located at $N = 4$.

In Fig. 3 we present the dependences of the relative errors ε'_T (Fig. 3a) and ε'_M (Fig. 3b) on the maximum b-value for different numbers N of data points. As seen in Fig. 3, positions of the minima in ε'_T and ε'_M are shifting to higher values of b_{max} with increasing N (the same is true for ε'_L and ε'_A as well). Values of ε'_j depend non-monotonically on N; thus, there are *global* minima of ε'_j as functions of the two variables: b_{max} and N. Values of the pairs $\{b_{max}, N\}$ at

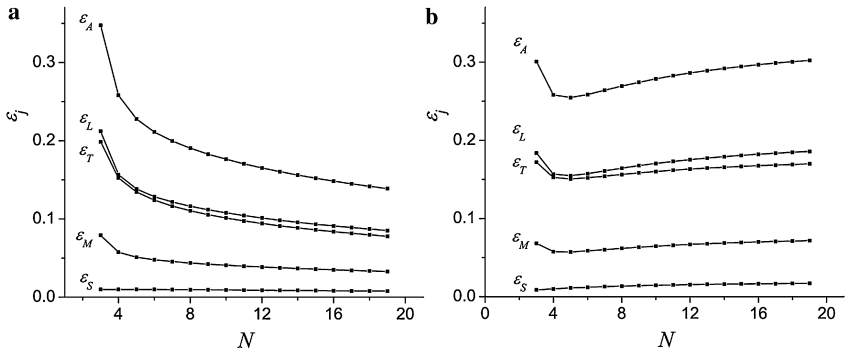

Fig. 2. The relative errors as functions of the number N of data points for fixed $b_{max} = 10$ s/cm^2, and the default values of other parameters. (a) The SNR is independent of N, Eq. (6), SNR = 100. (b) The SNR is inversely proportional to $\sqrt{N}$, Eq. (10), $SNR_0 = 200$.

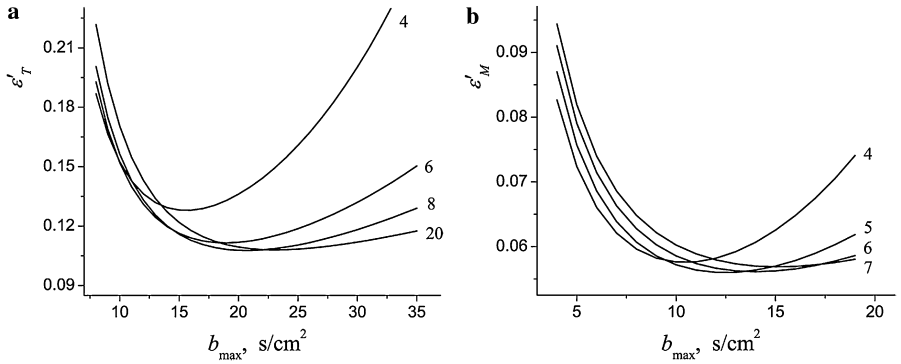

Fig. 3. The relative errors ε'_T (a) and ε'_M (b) as functions of b_{max} for different numbers N of data points (shown by the numbers near the curves). The default values of the diffusion parameters are assumed; $SNR_0 = 200$.

which the global minima occur can be found numerically for any given set of the diffusion parameters (see Section 5).

4. Validity of the approach: numerical simulations

As described in Appendix, the Laplace approximation is used for evaluating the integrals in Eq. (4). As a result, the marginal posterior probability distributions for the parameters $\{p_j\}$ were obtained in the Gaussian form, Eq. (5). However, the Laplace approximation is valid only under certain conditions.

First, our model breaks down in the limit when the longitudinal and transverse diffusion constants are close to one another, so that the diffusion anisotropy tends to 0. Formally, if $\hat{D}_A = 0$, the quantity I_{123} given by Eq. (24) tends to 0 and the functions U_j tend to infinity. This is a general problem of the method used above; it was discussed in detail in [19] for the example of the biexponential signal. In our model, in the case $\hat{D}_L = \hat{D}_T$ ($\hat{D}_A = 0$), the signal $S(b)$ is also reduced to a single-exponential function, see Eq. (13), and the peak in the joint posterior probability becomes a ridge line. As a consequence, the Laplace approximation is not valid and the given formulas do not apply.

Second, the validity of the Laplace approximation requires a high signal-to-noise ratio, so that the high order expansion terms can be ignored [19]. To illustrate this statement, we evaluated the marginal posterior probability densities $P(p_j|D\sigma I)$ numerically, without using the Laplace approximation, for different values of the parameter σ. The probability distributions for the transverse diffusivity D_T and the diffusion anisotropy D_A are shown in Fig. 4 for $\hat{D}_L = 0.4\ \mathrm{cm}^2/\mathrm{s}$, $\hat{D}_T = 0.1\ \mathrm{cm}^2/\mathrm{s}$, $\hat{S}_0 = 1$, $N = 6$, $b_{max} = 10\ \mathrm{s}^2/\mathrm{cm}$ and three values of the SNR: 100, 50, and 25. The black lines correspond to numerical integration in Eq. (4) over the parameters D_A and S_0 for $P(D_T|D\sigma I)$ and over D_T and S_0 for $P(D_A|D\sigma I)$; the red lines represent the probability distributions obtained by means of the Laplace approximation, Eqs. (5) and (6).

The analytical predictions for the standard deviations σ_j and relative errors ε_j given by Eq. (6) were also compared with the results of computer simulations and frequency-of-occurence analysis (histogram). For this, Gaussian noise was added to ideal data from Eq. (1) with known $\hat{D}_A, \hat{D}_T$ and $\hat{S}_0$; this generated data set was then analyzed according to Eq. (1) to get the apparent values of D_A, D_T and S_0 as well as their linear combinations: $D_L = D_T + D_A$ and the mean diffusivity $D_M = (D_L + 2D_T)/3$. This procedure was repeated 6×10^4 times. The procedure of fitting Eq. (1) to each generated data set was executed in two ways: by standard χ^2—minimization and by the Bayesian approach. The latter gives (for each set of generated data) two values of each estimated parameter—the peak value and the mean value. Comparison of the two estimates illustrates that the peak values of the estimated parameters obtained by the Bayesian approach practically coincide with the corresponding values obtained by χ^2—minimization. The peak and mean values of the parameters D_T and D_A obtained by the Bayesian approach for 6×10^4 generated data sets were statistically analyzed; the normalized frequency distributions (frequency-of-occurrence histograms) of the parameters are shown in Fig. 4 by blue and green dots, respectively. All the distributions are normalized to yield a total area of unity under the curve.

As evident in Fig. 4, for SNR = 100 the probability distributions $P(D_T|D\sigma I)$ and $P(D_A|D\sigma I)$ obtained by the numerical integration (black lines) have a typical Gaussian form with the maxima at the input values of the diffusion parameters ($\hat{D}_L = 0.4\ \mathrm{cm}^2/\mathrm{s}$ and $\hat{D}_T = 0.1\ \mathrm{cm}^2/\mathrm{s}$). The exact probability distributions practically coincide with the distributions obtained in the Laplace approximation (red lines). From the 6×10^4 generated data sets with $SNR = 100$, the frequency-of-occurrence histogram of both the mean and peak values demonstrate excellent agreement with $P(D_T|D\sigma I)$ and $P(D_A|D\sigma I)$.

For SNR = 50, the deviation between the probability distribution obtained by numerical integration and that calculated in the Laplace approximation is more pronounced. The frequency-of-occurrence histograms for the peak values (blue dots) reveal additional maxima located at the same values where the curves corresponding to the exact integration deviate from the Gaussians: at $D_T \approx 0.17\ \mathrm{cm}^2/s$ for the transverse diffusivity and at $D_A = 0$ for the diffusion

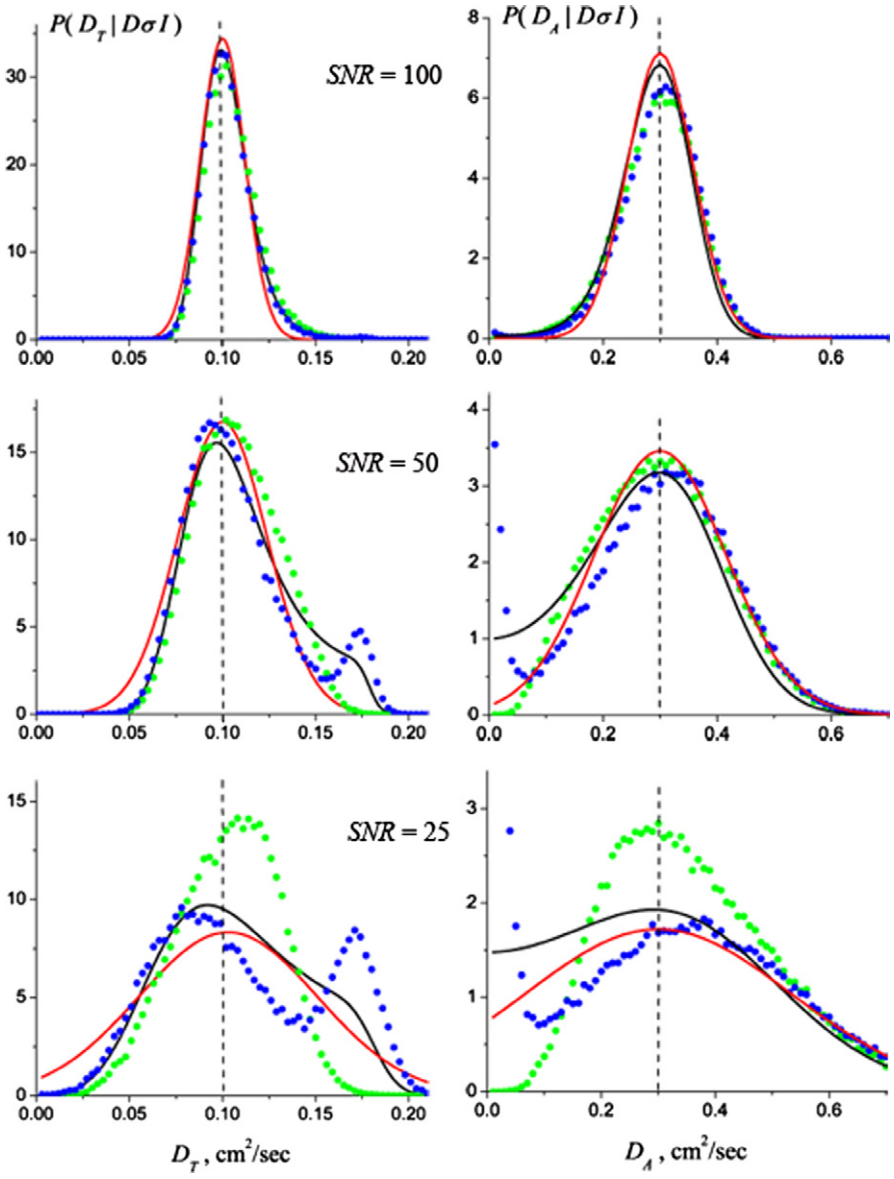

Fig. 4. The posterior probability distributions $P(D_T|D\sigma I)$ (left panels) and $P(D_A|D\sigma I)$ (right panels) for $\hat{D}_L = 0.4\,cm^2/s$, $\hat{D}_T = 0.1\,cm^2/s$, $N = 6$, $b_{max} = 10\,s^2/cm$ and $SNR = 100, 50, 25$. Black lines correspond to numerical integration in Eq. (4); red lines represent the Laplace approximation. Blue and green dots represent the normalized frequency distributions (frequency-of-occurrence histogram) of the peak and mean values of the parameters, respectively, obtained by the Bayesian analysis of each of 6×10^4 generated data sets. Vertical dashed lines indicate the input (''true'') values.

anisotropy. However, the histograms for the mean values of the estimated parameters (green dots) have no such maxima and remain in good agreement with the Laplace approximation.

For SNR = 25, the result of the Laplace approximation substantially deviates from the numerical integration, for which the distribution of $P(D_T|D\sigma I)$ is substantially non-Gaussian. However, even for this low SNR, the half-width of the probability distribution $P(D_T|D\sigma I)$ turns out to be rather close to that of the Gaussian curve and Eq. (6) provides a reasonable estimate for ε_T. The positions of the central maxima in the frequency-of-occurrence histograms for the peak values deviate from the input values. However, it is rather interesting (and unexpected) that the maxima of the histogram of the mean values of the estimated parameters are only slightly shifted from the input values. This demonstrates that the mean values obtained from the Bayesian analysis should be used for better estimation of diffusion parameters at low SNR, compared to the peak values or the values from χ^2—minimization (since these last two measures practically coincide as remarked above).

5. Discussion

In the graphs shown in Figs. 1 and 2, we used default values of the ''true'' diffusion coefficients ($\hat{D}_L = 0.4\,cm^2/s$ and $\hat{D}_T = 0.1\,cm^2/s$) characteristic of healthy human lungs. In emphysematous lungs, the size of the airways increases,

diffusion becomes less restricted and the parameter $\hat{D}_T$ increases. In extremely damaged parts of lungs, gas diffusion becomes practically unrestricted and nearly isotropic ($\hat{D}_A \to 0$, $\hat{D}_{L,T} \to D_0$) and can therefore be described by a single diffusion coefficient close to the free diffusion coefficient D_0. In this case, the model with three independent parameters becomes redundant and the signal can be described by a monoexponential function with two independent parameters. It means that our results are applicable to healthy lungs or lungs with initial stages of emphysema, when the difference between longitudinal and transverse diffusivity is substantial. For lungs with severe emphysema, another model of gas diffusion should be considered.

The behavior of the relative errors as functions of b_{max}, Fig. 1a, can be explained as follows. In this case, with fixed N, the b_{max}-dependence of the relative errors is affected by two opposite tendencies. On one hand, very small b-values produce only small amounts of signal attenuation. Such data sets are extremely insensitive to the diffusion coefficients and result in large errors (except for S_0; if b_{max} is very small and bD_T, $bD_L \ll 1$, all N data points serve mainly to determine the unattenuated signal amplitude S_0). On the other hand, overly high b-values (bD_T, $bD_L \gg 1$) attenuate the signal below noise level and provide no information. When the maximum b-value is small, the first argument dominates and the relative errors ε_j decrease with increasing b_{max}; however, for very large b_{max}, the second tendency becomes dominant and ε_j increases with increasing b_{max}. Note also that the quantity ε_M is substantially smaller than the relative errors corresponding to the other diffusion parameters. The mean diffusivity is the best-estimated parameter because D_M determines the initial slope of the signal, $S(b)/S_0 = 1 - bD_M + O(b^2)$ while D_A (or D_L, D_T as its linear combinations) appears only in the higher terms of the expansion with respect to b and, therefore, primarily influences the large-b tail of the decay curve $S(b)$ of Fig. 1b.

A monotonic decrease of ε_j with increasing N for fixed b_{max}, Fig. 2a, reflects the simple fact that any additional information diminishes the estimation errors. However, as mentioned above, such a dependence of the relative errors takes place in the case when the SNR is independent of N. For hyperpolarized ^{3}He imaging with a fixed bolus of gas to yield all N images, when the unattenuated signal amplitude and SNR decrease (being inversely proportional to $\sqrt{N}$, Eq. (9)) as N increases, the modified expressions for the errors, Eq. (10), should be used. In this case, the N-dependences of ε'_j corresponding to the diffusion parameters have minima at certain N depending on b_{max}.

As demonstrated in Fig. 3, with increasing N, the minima of the relative errors ε'_j as functions of the maximum b-value are shifting toward higher values of b_{max}. In addition, the ε'_j as functions of two parameters—b_{max} and N—have global minima at certain values of these variables. For the default values of the "true" diffusion parameters, the pairs $\{b_{max}, N\}$, at which the global minima occur, are as follows: $\{22\ \mathrm{s/cm^2}, 11\}$, $\{18\ \mathrm{s/cm^2}, 7\}$, $\{13\ \mathrm{s/cm^2}, 5\}$, $\{19\ \mathrm{s/cm^2}, 8\}$ for ε'_T, ε'_L, ε'_M, ε'_A, respectively. Clearly, lower uncertainties in the estimated diffusion parameters can be achieved by selecting b_{max} and N near these global minima.

Let us consider an example. In the previous experimental study [5], the pulse sequence with $N = 6$ and $b_{max} = 7.6\ \mathrm{s/cm^2}$ was used. For diffusion parameters, $\hat{D}_L = 0.4\ \mathrm{cm^2/s}$, $\hat{D}_T = 0.1\ \mathrm{cm^2/s}$, and SNR = 100, the relative error for the transverse diffusivity, calculated by means of Eq. (6), is equal to $\varepsilon_T = 0.17$. On the other hand, according to Eq. (6) for these parameters the minimum of ε_T can be achieved at a substantially higher $b_{max} = 19\ \mathrm{s/cm^2}$ for which $\varepsilon_T = 0.09$. Thus, our theory predicts that one could gain a doubled accuracy in determining the transverse diffusivity by using higher b_{max}, if the signal remains higher than the noise level (see Fig. 1b). It should be noted, however, that the optimal value of b_{max} significantly depends on the "true" values of the diffusivities that are usually unknown and can vary substantially even in the same patient. For example, in the ongoing experiments in our laboratory, the values of $\hat{D}_L$ and $\hat{D}_T$ across patients (and even for the same patient) are spread over the broad intervals (0.35–0.7) and (0.04–0.14) $\mathrm{cm^2/s}$, respectively. Because they are not a priori known, caution should be exercised in selecting the maximum b-value to maintain the signal in all voxels above the noise level. For example, to maintain the signal at the level $S(b_{max})/S_0 > 0.1$ for the highest values of $\hat{D}_{L,T}$, $\hat{D}_L = 0.7\ \mathrm{cm^2/s}$, $\hat{D}_T = 0.14\ \mathrm{cm^2/s}$, we need to restrict the pulse sequence to $b_{max} = 10\ \mathrm{s/cm^2}$, for which the relative error, $\varepsilon_T = 0.089$, remains very close to its minimum value $\varepsilon_T = 0.086$ at $b_{max} = 12\ \mathrm{s/cm^2}$. For the smallest values of the diffusivities, $\hat{D}_L = 0.35\ \mathrm{cm^2/s}$, $\hat{D}_T = 0.04\ \mathrm{cm^2/s}$, however, the relative error becomes much higher, $\varepsilon_T = 0.21$. Hence increased SNR is required to achieve rather small errors for both small and high diffusivities. However, in the experiment where preliminary estimates of transverse and longitudinal diffusivities are available, substantial improvement (factor of 2 in above example) in parameter estimation can be achieved by selecting the proper maximum b-values.

It is also worth noting that the locations of the minima of the relative errors corresponding to the different parameters (D_L, D_T, D_M, D_A) are different. This result is important for pulse sequence design: if the mean diffusivity D_M is of primary interest, one should use much smaller b-values and a smaller number N of b-values than in the case where the separate values of the longitudinal and transverse diffusivities are targeted.

It should be emphasized that in the approach described above a high signal-to-noise ratio is assumed. Thus, our results for the parameter estimates should be considered as a lower bound on the estimated uncertainties. The actual parameter estimates obtained for any given data set will essentially never be better than these estimates, and will almost certainly be worse.

The traditional way to obtain lower bounds on parameter estimates is using the Cramer–Rao lower bound. The

Cramer–Rao lower bound is a theoretical result that specifies the minimum variance for a parameter estimate, given an unbiased, single parameter estimator [22,23]. However, the Cramer–Rao lower bound does not provide the estimator; the latter must be guessed and then tested to see if it achieves the Cramer–Rao lower bound. The Cox theorem [24, Chapters 1–3] guarantees that the Bayesian estimate is the best estimate one can make. Any other technique will either do worse, or reproduce the Bayesian results, but it will not outperform the Bayesian calculation.

The calculations presented here are made for a specific example of signal dependence on the b-value, Eqs. (1) or (13). However, this method of estimating the uncertainties and relative errors, based on the Bayesian approach, can be readily generalized to a signal with different functional dependence (or, e.g., on acquisition time) and a different number of parameters. In the case of M parameters, the coefficients g_{jk} in the expansion of the function Q (see Eq. (17)) form a symmetric square matrix $\mathbf{G}$ of dimensionality $M \times M$, and the integration over $(M-1)$ parameters (similar to Eq. (4)) leads to the marginal posterior probability density of the remaining parameter, Eq. (22), where the sought standard deviation will be proportional to

$$\sigma_j \sim \left[\frac{\Delta_j}{\Delta}\right]^{1/2}, \tag{12}$$

where $\Delta = \det \mathbf{G}$ and Δ_j is the complementary minor of the diagonal element g_{jj} in the matrix $\mathbf{G}$.

6. Conclusion

The Bayesian analysis approach is used herein for analyzing the uncertainties in the parameter estimates in the model of ^{3}He gas diffusion in acinar airways. The uncertainties for the transverse diffusivity, diffusion anisotropy, and signal amplitude are analyzed as functions of the "true" values of the parameters, the signal-to-noise ratio, the maximum b-value and the total number of b-values used in the experiment. It is shown that for a given set of the "true" diffusion parameters, the dependences of the relative errors of the diffusion coefficients on the maximum b-value and total number of data points (b-values) have minima. Choosing MR pulse sequence parameters corresponding to these minima optimizes the diffusion MR experiment and gives the best possible estimate of the diffusion coefficients, providing that the signal-to-noise ratio is sufficiently high to ensure the signal for all b-values remains higher than the noise level. The mathematical approach can be generalized for models containing arbitrary numbers of parameters to be estimated.

Acknowledgment

This work was supported by NIH Grant R01 HL 70037.

Appendix

To obtain the marginal posterior probability $P(p_j|D\sigma I)$ for each of the parameter p_j, we need to calculate the sum in the function Q (see Eq. (3)) and then to integrate the joint posterior probability $P(\{p_j\}|D\sigma I)$ over the two other parameters.

When the signal as a function of b-value is described by a one- or a sum of two-exponential function, the sum in Eq. (3) can be easily calculated as a geometric progression [19]. To perform such a summation in our model, we rewrite the signal $S(b)$ (1) in the integral form:

$$S(b) = S_0 \cdot \exp\left(-b \cdot D_{\mathrm{T}}\right) \cdot \int_0^1 \mathrm{d}x \exp\left(-b \cdot D_{\mathrm{A}} x^2\right). \tag{13}$$

Substituting Eq. (13) into Eq. (3), the quantity Q can be written as

$$\begin{aligned} Q = {} & S_0^2 \cdot \int_0^1 \int_0^1 \mathrm{d}x\,\mathrm{d}y \cdot \Sigma(r_1(x,y)) \\ & - 2S_0\hat{S}_0 \cdot \int_0^1 \int_0^1 \mathrm{d}x\,\mathrm{d}y \cdot \Sigma(r_2(x,y)) \\ & + \hat{S}_0^2 \cdot \int_0^1 \int_0^1 \mathrm{d}x\,\mathrm{d}y \cdot \Sigma(r_3(x,y)), \end{aligned} \tag{14}$$

where

$$\begin{aligned} r_1(x,y) &= 2D_{\mathrm{T}} + D_{\mathrm{A}}(x^2+y^2), \\ r_2(x,y) &= D_{\mathrm{T}} + \hat{D}_{\mathrm{T}} + D_{\mathrm{A}}x^2 + \hat{D}_{\mathrm{A}}y^2, \\ r_3(x,y) &= 2\hat{D}_{\mathrm{T}} + \hat{D}_{\mathrm{A}}(x^2+y^2), \end{aligned} \tag{15}$$

and

$$\begin{aligned} \Sigma(r_i) &= \sum_{n=0}^{N-1} \exp\left(-r_i b_n\right) = \frac{1-\exp\left(-r_i\bar{b}\right)}{1-\exp\left(-r_i\Delta b\right)}, \\ \bar{b} &= N\Delta b = b_{\max} \cdot \left(\frac{N}{N-1}\right). \end{aligned} \tag{16}$$

As compared to [19], however, we do not assume that (i) the signal has "died" when the b-value reaches its maximum value $b_{\max} = \Delta b \cdot (N-1)$; (ii) the b-value increment Δb is small and $\Delta b \cdot r_i \ll 1$. Thus, we do not neglect the exponential term in the numerator in Eq. (16) and do not expand the denominator in a series with respect to $\Delta b \cdot r_i$, making it possible to analyze how the uncertainties of the estimated parameters depend on the number N of data points N for any $N \geqslant 3$.

The quantity Q is a very complicated function of the parameters p_j and the integrals (4) can not be evaluated in a closed form. However, the integrand in Eq. (4) is expected to have a sharp maximum at $p_j = \hat{p}_j$. Therefore, the integrals (4) can be calculated in the Laplace approximation (the real version of the method of stationary phase in complex analysis), in which the function Q is approximated by its Taylor expansion around the minimum with respect to all the parameters p_j up to the second order:

$$Q \approx \text{const} + \sum_{i,k=1}^{3} g_{ik}(p_i - \hat{p}_i)(p_k - \hat{p}_k) \tag{17}$$

(it is easy to verify that the first-order terms in the expansion are equal to 0). The coefficients $g_{ik} = g_{ki}$ in Eq. (17) can be obtained from Eqs. (14)–(16). After some algebra, we get

$$g_{ik} = \hat{S}_0^{m_{ik}} I_{ik}(D_A, D_T, \Delta b, N), \tag{18}$$

where $m_{11} = 0,\ m_{12} = m_{13} = 1,\ m_{22} = m_{33} = m_{23} = 2$. The functions I_{ik} and f_{ik} are

$$I_{ik}(D_A, D_T, \Delta b, N) = \int_0^1 \int_0^1 \mathrm{d}x\,\mathrm{d}y f_{ik}(x,y) \; v_{m_{ik}}(D_A, D_T, \Delta b, N; x, y), \tag{19}$$

$$v_0 = \frac{1 - \exp(-\bar{b}\lambda)}{1 - \exp(-\Delta b\lambda)},$$

$$v_1 = \frac{\exp(-b_{\max}\lambda)}{[\exp(\Delta b\lambda) - 1]^2} \cdot \left[\bar{b}(\exp(\Delta b\lambda) - 1) - \Delta b\left(\exp(\bar{b}\,\lambda) - 1\right)\right],$$

$$v_2 = \frac{\exp(-b_{\max}\lambda)}{[\exp(\Delta b\lambda) - 1]^3} \cdot \Big[\Delta b^2(\exp(\Delta b\lambda) + 1)\left(\exp(\bar{b}\lambda) - 1\right). \\ -\bar{b}^2(\exp(\Delta b\lambda) - 1)^2 - 2\bar{b}\Delta b\left(\exp(\bar{b}\lambda) - 1\right)\Big], \tag{20}$$

$$\lambda \equiv \lambda(D_A, D_T; x, y) = 2\hat{D}_T + \hat{D}_A(x^2 + y^2),$$

$$f_{11} = f_{33} = f_{13} = 1, \quad f_{12} = f_{23} = y^2, \quad f_{22} = x^2 y^2. \tag{21}$$

As the function Q is reduced to the symmetric and positive-defined quadratic form (15) with respect to the differences $(p_j - \hat{p}_j)$, the integration in Eq. (4) over two of three parameters $\{p_j\}$ can be readily achieved resulting in the marginal posterior probability density for the parameters p_j in the Gaussian form:

$$P(p_j | D\sigma I) \propto \exp\left(-\frac{(p_j - \hat{p}_j)^2}{2\sigma_j^2}\right), \tag{22}$$

where σ_j are the width of the posterior probability in the Laplace approximation,

$$\sigma_j = \varepsilon_j \hat{p}_j, \qquad \varepsilon_j = \frac{1}{\mathrm{SNR}} \cdot U_j(\hat{D}_A, \hat{D}_T, \Delta b, N). \tag{23}$$

Here the ε_j are the desired relative errors of the parameter estimates, $\mathrm{SNR} = \hat{S}_0/\sigma$ is the signal-to-noise ratio; U_j are functions of the integrals I_{ik} given by Eqs. (19)–(21):

$$U_1(\hat{D}_A, \hat{D}_T, \Delta b, N) = \left[\frac{I_{22}I_{33} - I_{23}^2}{I_{123}}\right]^{1/2},$$

$$U_2(\hat{D}_A, \hat{D}_T, \Delta b, N) = \frac{1}{\hat{D}_A} \cdot \left[\frac{I_{11}I_{33} - I_{13}^2}{I_{123}}\right]^{1/2}, \tag{24}$$

$$U_3(\hat{D}_A, \hat{D}_T, \Delta b, N) = \frac{1}{\hat{D}_T} \cdot \left[\frac{I_{11}I_{22} - I_{12}^2}{I_{123}}\right]^{1/2},$$

and

$$I_{123} = I_{11}I_{22}I_{33} + 2I_{12}I_{13}I_{23} - I_{11}I_{23}^2 - I_{22}I_{13}^2 - I_{33}I_{12}^2. \tag{25}$$

If the b-value increment Δb is small enough so that $\Delta b \cdot \hat{D}_T < 1,\ \Delta b \cdot \hat{D}_A < 1$ as generally occurs, the expressions for ε_j can be simplified and re-written in the form

$$\varepsilon_j = \frac{1}{\mathrm{SNR} \cdot \sqrt{N}} \cdot V_j(B_A, B_T), \tag{26}$$

where $V_j(B_A, B_T)$ depend only on two dimensionless parameters $B_A = \bar{b}\hat{D}_A,\ B_T = \bar{b}\hat{D}_T$. For sufficiently large N, the functions V_j become independent of N, and the relative errors ε_j turn out to be inversely proportional to $\sqrt{N}$.

References

[1] G.L. Snider, Distinguishing among asthma, chronic bronchitis, and emphysema, Chest 87 (1985) 35S–39S.

[2] X.J. Chen, L.W. Hedlund, H.E. Moller, M.S. Chawla, R.R. Maronpot, G.A. Johnson, Detection of emphysema in rat lungs by using magnetic resonance measurements of 3He diffusion, Proc. Natl. Acad. Sci. USA 97 (2000) 11478–11481.

[3] B.T. Saam, D.A. Yablonskiy, V.D. Kodibagkar, J.C. Leawoods, D.S. Gierada, J.D. Cooper, S.S. Lefrak, M.S. Conradi, MR imaging of diffusion of (3)He gas in healthy and diseased lungs, Magn. Reson. Med. 44 (2000) 174–179.

[4] M. Salerno, E.E. de Lange, T.A. Altes, J.D. Truwit, J.R. Brookeman, J.P. Mugler 3rd, Emphysema: hyperpolarized helium 3 diffusion MR imaging of the lungs compared with spirometric indexes–initial experience, Radiology 222 (2002) 252–260.

[5] D.A. Yablonskiy, A.L. Sukstanskii, J.C. Leawoods, D.S. Gierada, G.L. Bretthorst, S.S. Lefrak, J.D. Cooper, M.S. Conradi, Quantitative *in vivo* assessment of lung microstructure at the alveolar level with hyperpolarized ^{3}He diffusion MRI, Proc. Natl. Acad. Sci. USA 99 (2002) 3111–3116.

[6] G. Peces-Barba, J. Ruiz-Cabello, Y. Cremillieux, I. Rodriguez, D. Dupuich, V. Callot, M. Ortega, M.L. Rubio Arbo, M. Cortijo, N. Gonzalez-Mangado, Helium-3 MRI diffusion coefficient: correlation to morphometry in a model of mild emphysema, Eur. Respir. J. 22 (2003) 14–19.

[7] A.J. Swift, J.M. Wild, S. Fichele, N. Woodhouse, S. Fleming, J. Waterhouse, R.A. Lawson, M.N. Paley, E.J. Van Beek, Emphysematous changes and normal variation in smokers and COPD patients using diffusion 3He MRI, Eur. J. Radiol. 54 (2005) 352–358.

[8] A.E. Morbach, K.K. Gast, J. Schmiedeskamp, A. Dahmen, A. Herweling, C.P. Heussel, H.U. Kauczor, W.G. Schreiber, Diffusion-weighted MRI of the lung with hyperpolarized helium-3: a study of reproducibility, J. Magn. Reson. Imaging 21 (2005) 765–774.

[9] S.B. Fain, T.A. Altes, S.R. Panth, M.D. Evans, B. Waters, J.P. Mugler 3rd, F.R. Korosec, T.M. Grist, M. Silverman, M. Salerno, J. Owers-Bradley, Detection of age-dependent changes in healthy adult lungs with diffusion-weighted 3He MRI, Acad. Radiol. 12 (2005) 1385–1393.

[10] J.R. Owers-Bradley, S. Fichele, A. Bennattayalah, C.J. McGloin, R.W. Bowtell, P.S. Morgan, A.R. Moody, MR tagging of human lungs using hyperpolarized 3He gas, J. Magn. Reson. Imaging 17 (2003) 142–146.

[11] J.C. Woods, D.A. Yablonskiy, K. Chino, T.S. Tanoli, J.D. Cooper, M.S. Conradi, Magnetization tagging decay to measure long-range (3)He diffusion in healthy and emphysematous canine lungs, Magn. Reson. Med. 51 (2004) 1002–1008.

[12] J.C. Woods, D.A. Yablonskiy, C.K. Choong, K. Chino, J.A. Pierce, J.C. Hogg, J. Bentley, J.D. Cooper, M.S. Conradi, P.T. Macklem, Long-range diffusion of hyperpolarized 3He in explanted normal and emphysematous human lungs via magnetization tagging, J. Appl. Physiol. 99 (2005) 1992–1997.

[13] C. Wang, G.W. Miller, T.A. Altes, E.E. de Lange, G.D. Cates Jr., J.P. Mugler 3rd, Time dependence of 3He diffusion in the human lung:

measurement in the long-time regime using stimulated echoes, Magn. Reson. Med. 56 (2006) 296–309.
[14] B. Haefeli-Bleuer, E.R. Weibel, Morphometry of the human pulmonary acinus, Anat. Rec. 220 (1988) 401–414.
[15] S. Fichele, M.N. Paley, N. Woodhouse, P.D. Griffiths, E.J. Van Beek, J.M. Wild, Finite-difference simulations of 3He diffusion in 3D alveolar ducts: comparison with the "cylinder model, Magn. Reson. Med. 52 (2004) 917–920.
[16] M. Paiva, Gaseous diffusion in an alveolar duct simulated by a digital computer, Comput. Biomed. Res. 7 (1974) 533–543.
[17] S. Verbanck, M. Paiva, Effective axial diffusion in an expansile alveolar duct model, Respir. Physiol. 73 (1988) 273–278.
[18] G.L. Bretthorst, Bayesian Spectrum Analysis and Parameters Estimation, Springer-Verlag, New York, 1988.
[19] G.L. Bretthorst, How accurately can parameters from exponential models be estimated? A Bayesian view, Concepts Magn. Reson. 27A (2005) 73–83.
[20] B. Saam, D.A. Yablonskiy, D.S. Gierada, M.S. Conradi, Rapid imaging of hyperpolarized gas using EPI, Magn. Reson. Med. 42 (1999) 507–514.
[21] M. Salerno, J.R. Brookeman, E.E. de Lange, J.P. Mugler, in: 11th ISMRM, Toronto, Canada, 2003, p. 1386.
[22] H. Cramer, Mathematical Method of Statistics, Princeton University Press, Princeton, NJ, 1946.
[23] C.R. Rao, Information and the accuracy attainable in the estimation of statistical parameters, Bull. Calcutta Math. Soc. 37 (1945) 81–91.
[24] E.T. Jaynes, Probability Theory: The Logic of Science, Cambridge University Press, Cambridge, 2003.